Development of Juvenile Scoliosis Spine FE Models to Understand Growth Rod Failure Mechanisms

October 2017

PI Name: Aakash Agarwal, PhD

Phone # 419-787-7689

Email: aakash.agarwal@utoledo.edu

Co PI Name: Vijay K. Goel, PhD

Phone # 419-530-8035

Email: vijay.goel@utoledo.edu

CDMI Trainee Name: Dikshya Parajuli, BE

Phone # 567-225-2464

Email: dikshya.parajuli@rockets.utoledo.edu

CDMI Trainee Name: Ardalan Seyed Vosoughi, MS

Phone # 571-420-4726

Email: ardalansv@gmail.com

Table of Contents

Background

Scoliosis is a complex spinal deformity having both abnormal lateral curvature and vertebral rotation. The clinical treatment of scoliosis depends on various factors, such as the severity of the deformity, the patient's age and remaining growth or progression of the deformation and location of the curve. The gold standard treatment for the pediatric patients is the use of growth rods. Growth rods provide the opportunity for the spine to grow in juvenile patients alongside preventing the progression of deformity. For this reason, the growth rods are becoming more popular for the juvenile patients as compared to traditional rods. However, there are many complications associated with growth rods. These complications include implant-related, fusion, alignment problems as well as skin-related and neurologic complications [1]. Growth rods exhibit failure and there is no standard method of evaluating the growth rods. Hence, our objectives are- to determine the biomechanical parameters that are prevalent with the failure of growth rods, and provide relevant testing methodology for standardization.

Aims

The aim of this study is divided into three different parts which includes- use of modified ASTM F1717 Compression bending test to validate our finite element (FE) approach, develop and validate FE models in generic and patient-specific scoliotic curves (data provided by FDA) and then perform parametric studies on configurations and materials.

Methods

Development of modified F1717 growing rod constructs

Five idealized F1717 constructs were developed where the component complexity was increased with use of various connectors and crosslinks at the superior and distal ends (Figure. 1). Rods were meshed using hexahedral elements (C3D8) while all other components were discretized with tetrahedral elements (C3D4). A tie constraint was used to bond all component interfaces. Adjacent to distal construct was also designed to represent clinical usage of components that has been associated with rod fracture [2]. The test blocks were modeled as UHMWPE (E = 690 MPa, ν= 0.46), while all device components were modeled as elasto-plastic titanium alloy, Ti6Al4V (E=105GPa, ν= 0.3 with isotropic hardening). To simulate compression-bending in each construct, 50mm displacement was applied at the center of the pin hole of the superior block and the construct was allowed to deform and rotate about the flexion-extension axis. We performed FE comparison of these constructs to validate FE output with the experimental data provided by FDA.

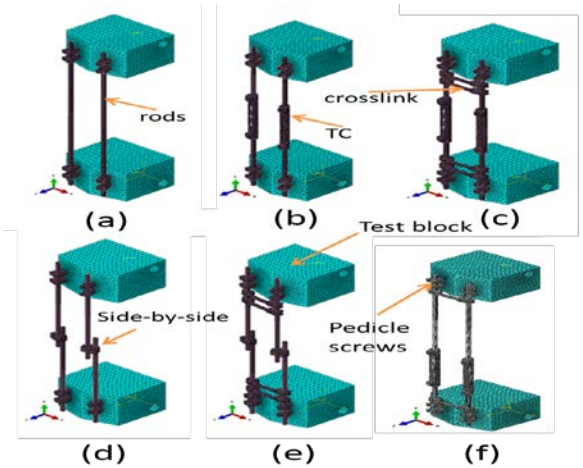

Figure 1. Modified ASTM F1717 Growth rod FE configurations. (a) Rods Only. (b) Long Tandem without cross connector. (c) Long Tandem with cross connector. (d) Side-by-side without cross connector. (e) Side-by-side with cross connector. (f) Adjacent to Distal construct.

Development of normal & representative scoliotic models with growth rod

Normal Juvenile Spine Model

A CT of a typical 9 year old juvenile patient was taken, and the vertebral body and intervertebral heights were recorded. Next a validated T1-S1 normal adult spine model [3] was scaled down to 71% of its original size to represent a juvenile size, based on literature data [4]. However, the vertebral body to intervertebral height ratio of an adult is very different to a juvenile spine. For this reason, the mesh of this scaled down normal spine finite element model was altered, using ABAQUS (Dassault Systèmes, Simulia Inc., Providence, RI), to personalize the vertebral body and intervertebral body height to that of the recorded heights from juvenile CT data (Figure 2). The material properties for the juvenile model were taken from the literature [4,5].

Figure 2. FE model of a normal juvenile spine after scaling and adjustment of vertebral body to intervertebral body heights.

Representative Juvenile Scoliotic Models

The above described normal juvenile spine model was used as a template to develop representative juvenile scoliotic models. The desired scoliotic spine was generated by using two custom script (MATLAB, Natick, MA UNITED STATES) that carried out the following operations: 1. Lateral shift to create coronal deformity and 2. Axial rotation to create axial deformity. In the lateral shift technique, we started with forming a polynomial equation of the form $X = f(Z) = a1+a2Z+a3Z\ 2+a4Z\ 3+….anZ\ n-1$, where X is the lateral shift (from the plum line), Z is the height (along the

length of the thoracolumbar spine), a1, a2,……. an are the coefficients of the equation and n-1 is the order of the equation. The curves defined by this polynomial equation were used as the base for projection of the normal spine finite element model. In the axial rotation technique, intervertebral discs (IVDs) and the vertebrae were rotated about the axis tangential to the sagittal profile line and passing through the center of the vertebral body or IVDs at that region. The angles of rotation for spine were taken from the literature [6].

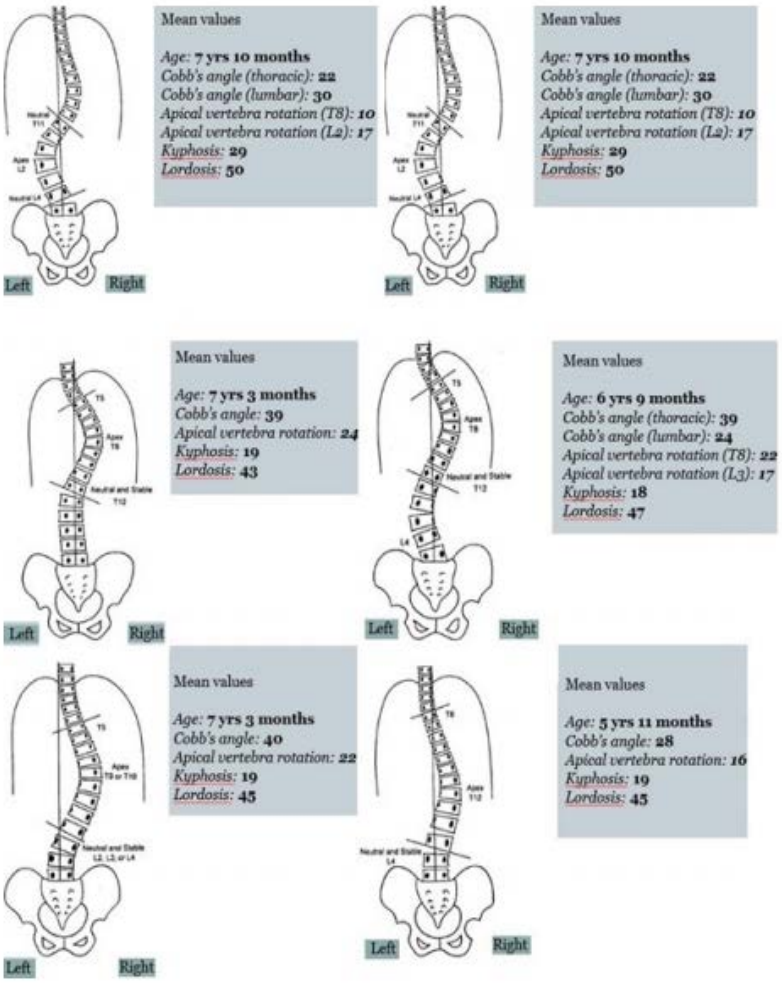

Figure 3. Various juvenile idiopathic curves as classified by Robinson et al [6] and used for generating representative scoliotic models.

Growth Rod Design and Instrumentation

Growth rod instrumentation for each model was designed using Solidworks (Dassault Systèmes SolidWorks Corporation, Waltham, MA). The growth rods were simulated in the FE spine models (normal and scoliotic) with eight 4.5 mm titanium alloy (Ti6Al4V) pedicle screws and four 4.5 mm titanium alloy (Ti6Al4V) rods (two distal and two proximal). The pedicle screws were kinematically coupled to the pedicles via bushings in all three degrees of freedom. The proximal rods were tied bilaterally to the respective ispilateral proximal pedicle screws and distal rods to ipsilateral distal pedicle screws. The tandem connection was simulated by kinematically coupling the ipsilateral free ends of the rods in all three degrees of freedom.

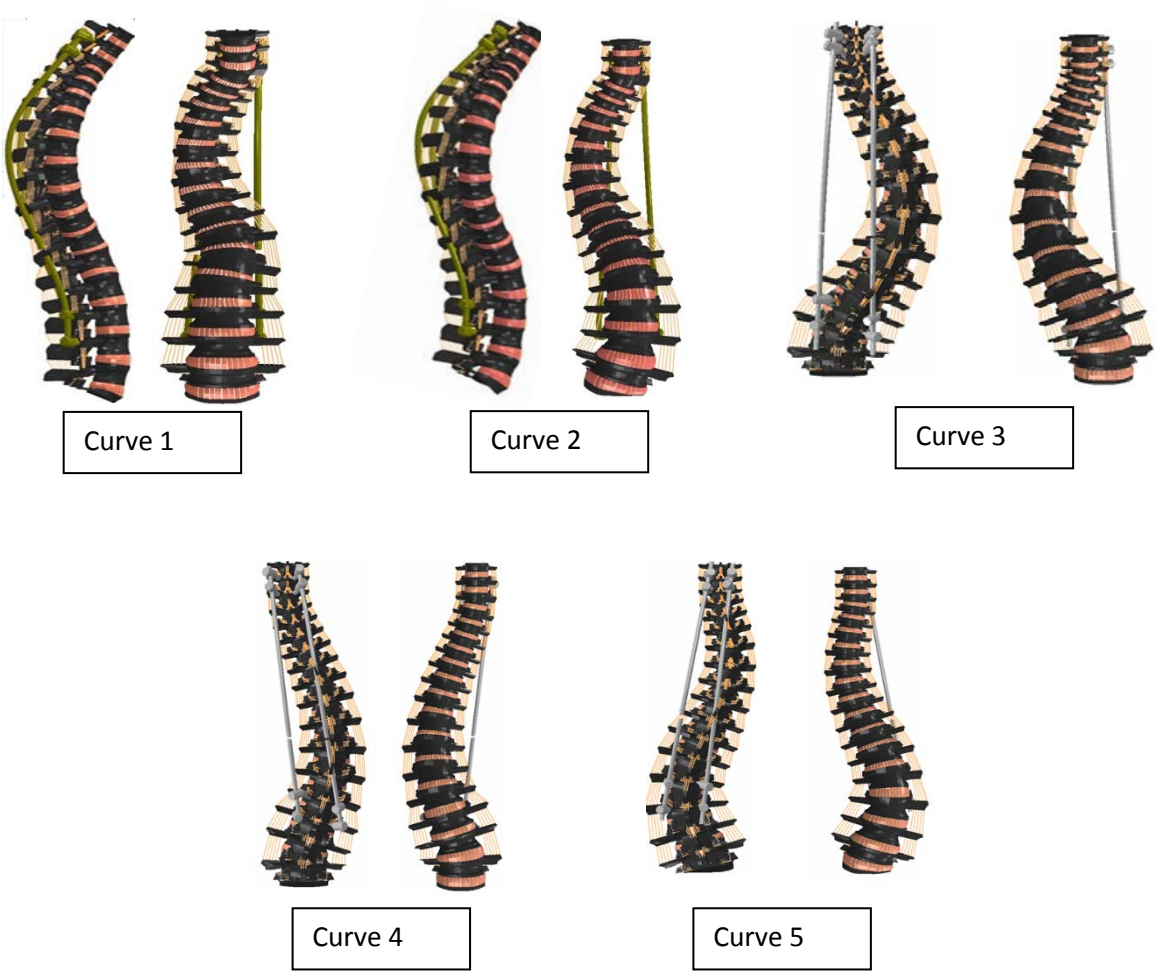

Figure 4. Representative scoliotic FE models.

Growth in the spine was incorporated using the Hueter-Volkmann principle which is expressed in the empirical equation below.

$$G = G"[1 + \beta(\sigma - \sigma")]$$

where G is the actual growth strain, G" is the mean baseline growth strain, σ is actual compressive stress on the growth plate, σ" is the mean baseline stress on the growth plate for the intact spine and β is equal to 1.5 MPa^{-1} for vertebrae. For intact model, G is equal to G". G" is equal to 0.035 per 6 months for a 9 year old child 58 spine, as per the published literature [7, 8]. Integration of this growth modulation into the FE model was done by means of thermal expansion, converting the growth strains (calculated from above equation for each element) into thermal loads and applying those across the nodes [9]. The thermal loads were determined using the following relation:

$$\delta T = \varepsilon/\alpha$$

where, δT is the thermal load for the iteration, ε is the thermal strain (growth strains) for the iteration, and α is an arbitrary number representing the coefficient of thermal expansion.

These FE models were used to analyze the effect of distraction forces on the load at bone-screw interface and stresses on the rods. Also, the effect of distraction frequencies on optimal distraction force and stresses on the rods were examined.

Results

Excellent agreement was obtained between the force-displacement curve predicted by FEA and measured experimentally for the five idealized construct configurations (Figure 5). The initial stiffness compared well between experiments and FEA, and the average percent difference in construct force across the entire curve was also low.

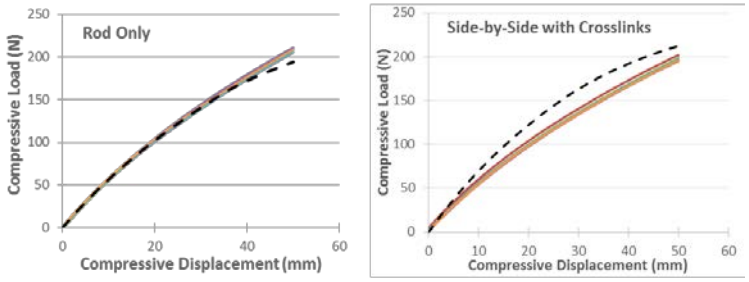

	Rod Only	Side-by-Side	Side-by-Side with Crosslink	Tandem Connector	Tandem Connector w/ crosslink	Clinically relevant
Stiffness (N/mm)	E: 5.9 C: 6.1	E: 6.4 C: 6.9N	E: 6.4 C: 7.6	E: 8.9 C: 9.8	E: 9.7 C: 11.3	E: C: 8.9
Avg force difference	1.5%	4.7%	16.6%	5.4%	9.2%	

Figure 5. Force-displacement curves for experiments (solid lines) and FE simulation (dashed line) for 2 of the idealized configurations. (**Experimental data provided by FDA**)

The FEA was also able to predict the force response in the clinically relevant construct configuration accurately when the component placement was precisely matched to the experiment (Figure 6).

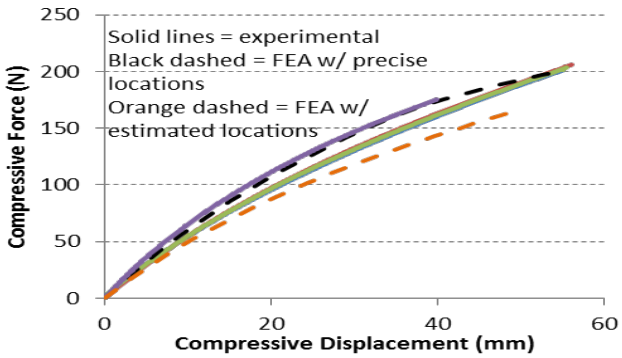

Figure 6. Force-displacement curve for experiments and FEA of clinically relevant configuration.

Effect of distraction force and distraction frequency on Normal Juvenile Spine

Figure 7 shows maximum von Mises stress in the growth rod after distraction and after 6 months of growth with different distraction forces. Immediately after distraction, the maximum von Mises stress on the rod increased unidirectonally from 50 to 400 N of distraction force. Also, the distraction force of 200-250 N resulted in the lowest maximum von Mises stress at 6 month postoperatively.

Figure 8 shows average load (N) at the screw-bone interface after distraction and after 6 months of growth. Similar loads were exerted on L4 and L5 vertebrae, but in the opposite direction. The average load at the screw-bone interface at the end of 6 months was lowest for 150, 200, and 250 N. The loads exerted increased bidirectionally with either an increase or decrease of distraction forces (i.e., either side of this range).

Figure 9 shows the maximum von Mises stress on the rod immediately after distraction with different frequencies of distraction for 24 months. The results indicate that the highest maximum von Mises stresses on the rod for the duration of 24 months decreased with an increase in the frequency of rod distraction.

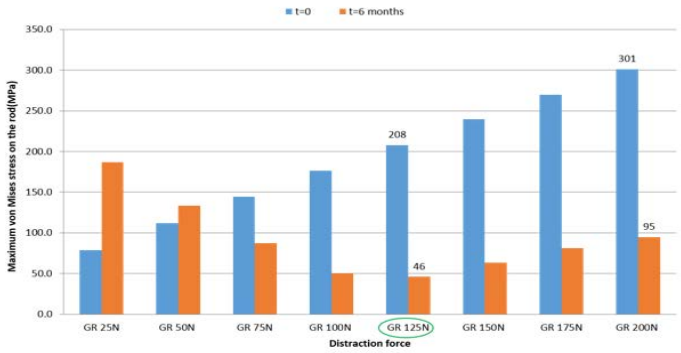

Figure 7. Maximum von Mises stress (in MPa) in the growth rod after distraction (t=0) and after 6 months of growth (t=6 months) with different distraction forces.

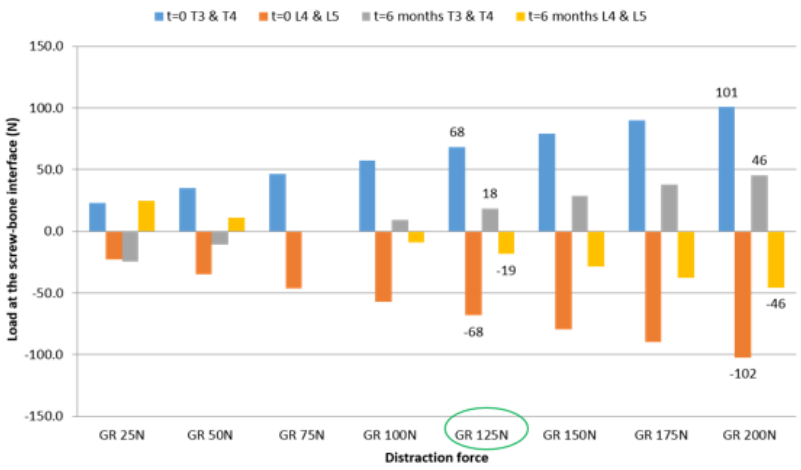

Figure 8. Average load (N) at the screw-bone interface after distraction (t=0) and after 6 months of growth (t=6 months) with different distraction forces. The positive values correspond to caudal-cranial direction and the negatives in cranial-caudal direction.

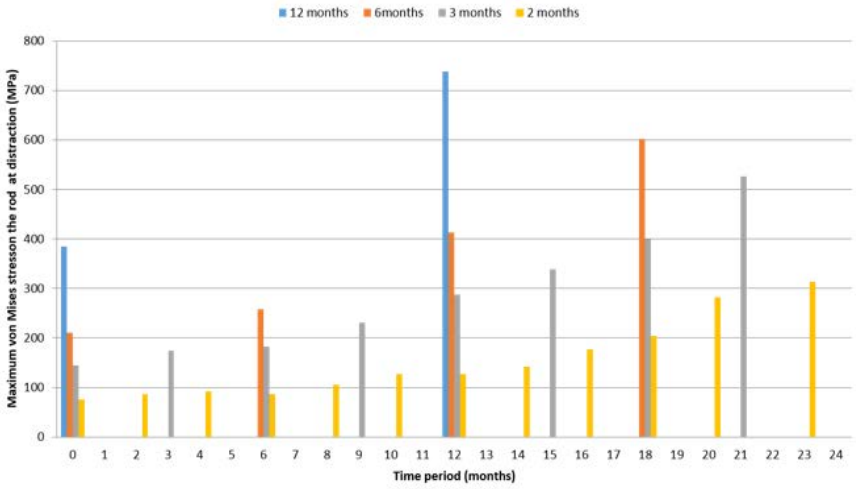

Figure 9. The graph shows the maximum von Mises stress on the rod immediately after distraction with different frequency of distraction for the duration of 24 months. For 12 monthly distraction there are two peaks (at 0 and at 12 months). For 6 monthly distraction there are four peaks (at 0, 6, 12, and 18 months). For 3 monthly distraction there are eight peaks (at 0, 3, 6, 9, 12, 15, 18, and 21 months). For 2 monthly distraction there are twelve peaks (at 0, 2, 4, 6, 8, 10, 12, 14, 16, 18, 20, and 22 months).

Effect of distraction force and distraction frequency on Representative Juvenile Spines

Figure 10 shows maximum von Mises stress in the growth rod after distraction and after 6 months of growth. The maximum von Mises stresses on the rods increased with increasing distraction forces, varying from 140 to 550 MPa.

Figure 11 shows average load (N) at the screw-bone interface after distraction and after 6 months of growth. The results followed the same trend.

Figure 12 shows the maximum von Mises stress on the rod immediately after distraction with different frequency of distraction for the duration of 24 months. For each distraction interval, the maximum von Mises stress on the rod increased at every successive distraction, however, the magnitude of stresses were lower for lower distraction intervals.

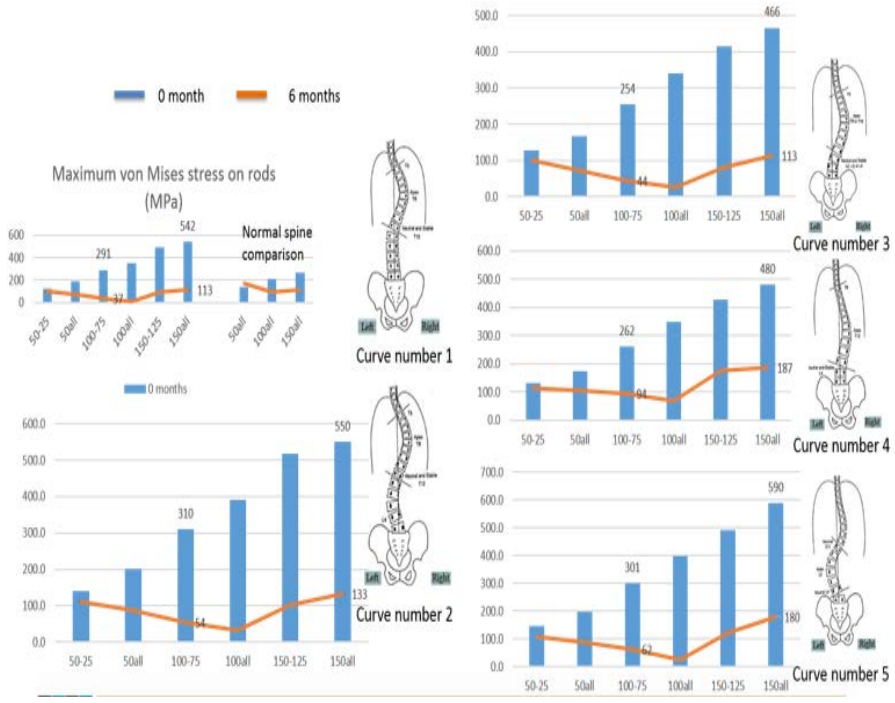

Figure 10. Maximum von Mises stress (in MPa) in the growth rod after distraction (t=0) and after 6 months of growth (t=6 months) for representative scoliotic models.

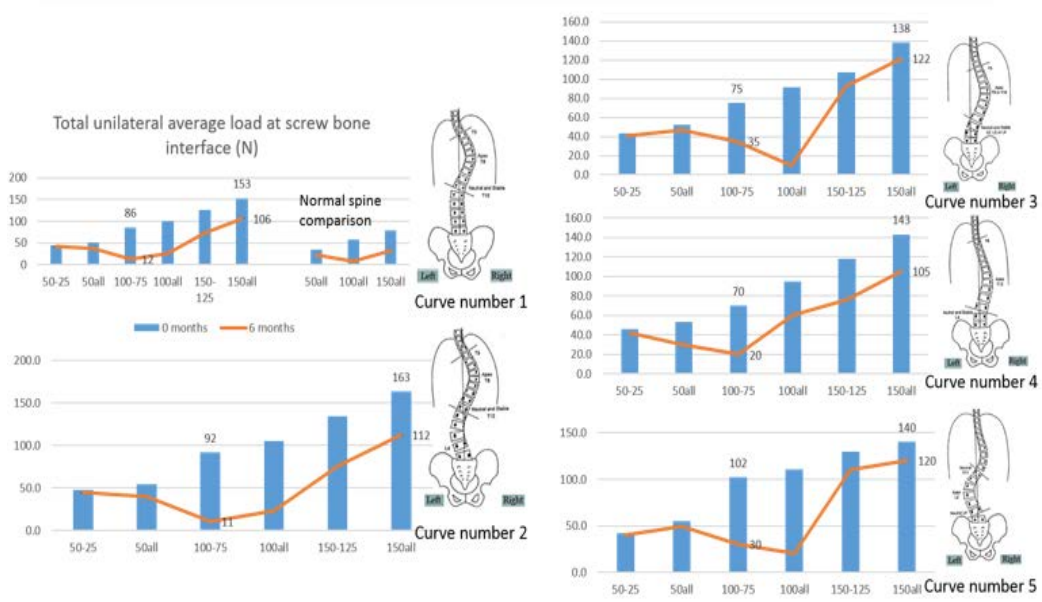

Figure 11. Total unilateral average load (N) at the screw-bone interface after distraction (t=0) and after 6 months of growth (t=6 months) for representative scoliotic models.

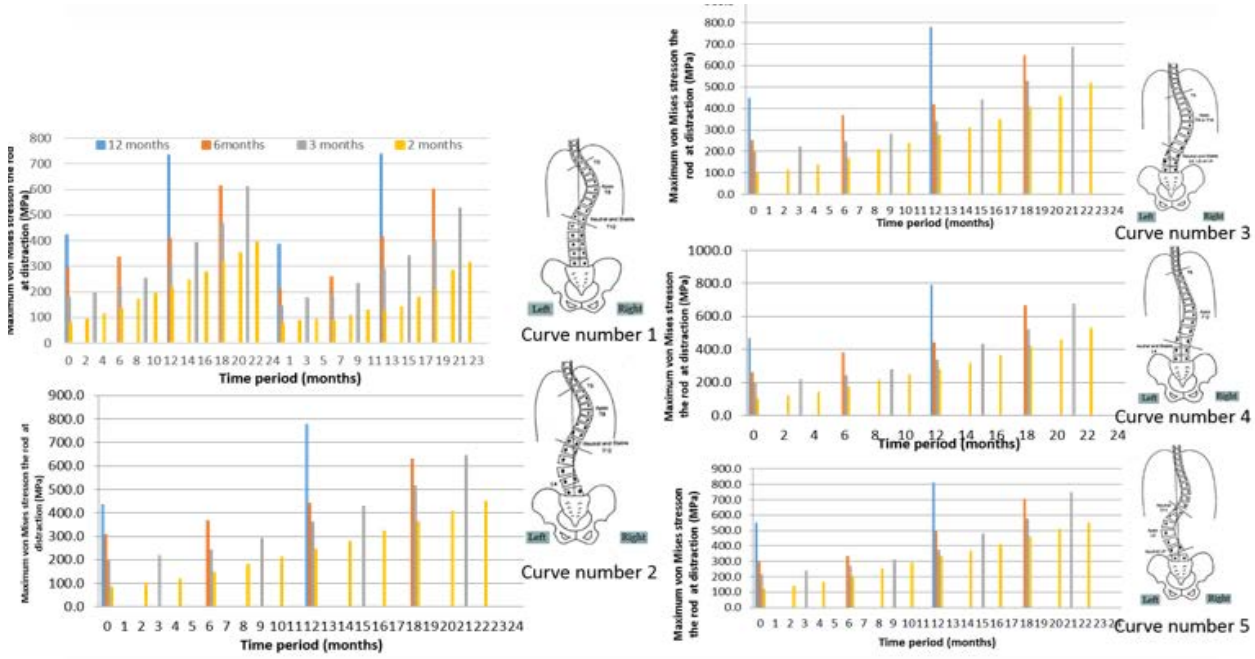

Figure 12. Maximum von Mises stress on the rod immediately after distraction with different frequency of distraction for the duration of 24 months.

Discussion and Conclusion

Mechanical characteristics for different constructs match the FDA experimental data. The validation of F1717 protocol is complete. The effects of distraction force on the loads at the screw-bone interface and maximum von Mises stresses on the rods were studied. In addition to that, the effects of frequency of distraction on maximum von Mises stresses on the rods for different loading conditions were also studied. Both normal and scoliotic juvenile spine models were chosen for the study. A normal juvenile spine model was first used to isolate the effect of distraction force and frequency on maximum von Mises stresses on the rods, thus producing results independent of the severity of deformity and curve rigidity. Next, multiple scoliotic spine models were developed to corroborate the trends in results observed using a normal juvenile spine. From these studies, we could see that an optimal distraction force exists with minimum stress on the rod and lower loads at screw-bone interface. The results of this study also signify the importance of shorter distraction period in reducing the stresses on the rods. Another observation was that higher distraction forces didn't produce stresses on rod or load on screw that could result in failure of the implant.

Future Work

For our future work, we will get the data from FDA to develop other patient specific scoliotic FE models and perform parametric studies. Results for patient specific FE models will be shared once we receive RIHSC Exemption from FDA Lab.

References

1. Yazici M, Olgun ZD. Growing rod concepts: state of the art. Eur Spine J. 2013;22:S118–30. doi: 10.1007/s00586-012-2327-7.

2. Hill et al 2017, Spine J, https://doi.org/10.1016/j.spinee.2017.04.020, In Press.

3. Palepu, V., Doctor of Philosophy Degree in Biomedical Engineering. 2013, The University of Toledo.

4. Kumaresan, S., et al., Biomechanical study of pediatric human cervical spine: a finite element approach. J Biomech Eng, 2000. 122(1): p. 60-71.

5. Jebaseelan DD, Jebaraj C, Yoganandan N, Rajasekaran S. Validation efforts and flexibilities of an eight-year-old human juvenile lumbar spine using a three-dimensional finite element model. Med Biol Eng Comput 2010;48:1223-31.

6. Robinson, C.M. and M.J. McMaster, Juvenile idiopathic scoliosis. Curve patterns and prognosis in one hundred and nine patients. J Bone Joint Surg Am, 1996. 78(8): p. 1140-8.

7. Stokes, I.A.F. and L. Windisch, Vertebral height growth predominates over intervertebral disc height growth in adolescents with scoliosis. Spine, 2006. 31(14): p. 1600-1604

8. Fok, J., S. Adeeb, and J. Carey, FEM Simulation of Non-Progressive Growth from Asymmetric Loading and Vicious Cycle Theory: Scoliosis Study Proof of Concept. Open Biomed Eng J, 2010. 4: p. 162-9.

9. Noordeen, H.M., et al., In Vivo Distraction Force and Length Measurements of Growing Rods: Which Factors Influence the Ability to Lengthen? Spine, 2011. 36(26): p. 2299.